HHS Public Access

Author manuscript

Nat Neurosci. Author manuscript; available in PMC 2013 September 26.

Published in final edited form as:

Nat Neurosci. 2013 March ; 16(3): 264–266. doi:10.1038/nn.3329.

Long-term dynamics of CA1 hippocampal place codes

Yaniv Ziv[1,*], **Laurie D. Burns**[1,*], **Eric D. Cocker**[1], **Elizabeth O. Hamel**[1], **Kunal K. Ghosh**[2], **Lacey J. Kitch**[1], **Abbas El Gamal**[2], and **Mark J. Schnitzer**[1,3,4]

[1]James H. Clark Center, Stanford University, Stanford CA 94305

[2]David Packard Electrical Engineering Building, Stanford University, Stanford CA 94305

[3]Howard Hughes Medical Institute, Stanford University, Stanford CA 94305

[4]CNC Program, Stanford University, Stanford CA 94305

Abstract

Via Ca^{2+}-imaging in freely behaving mice that repeatedly explored a familiar environment, we tracked thousands of CA1 pyramidal cells' place fields over weeks. Place coding was dynamic, for each day the ensemble representation of this environment involved a unique subset of cells. Yet, cells within the ∼15–25% overlap between any two of these subsets retained the same place fields, which sufficed to preserve an accurate spatial representation across weeks.

CA1 place cells are considered crucial for spatial memory, but data is limited regarding whether their representations of space evolve over time scales of weeks or more[1]. Some theories suggest place cells should retain stable place fields for long-term retention of familiar environments[1]. Alternatively, dynamic aspects of place coding may facilitate distinct memory traces of different events occurring in the same environment[2].

Due to technical limitations, it has been only partially explored if CA1 representations of familiar environments are stable or evolve over time. Electrical recordings from many tens of cells are feasible[3], but it is challenging to record from the same cells longer than a few days. Data on place fields' stability has largely been from small numbers of cells recorded over at most a week[4-10]. These studies have demonstrated cells with stable place fields, but the data have been too sparse to assess how coding evolves at the ensemble level.

To study long-term coding dynamics, we combined (Fig. 1a): a viral vector (AAV2/5-CamKIIα-GCaMP3) to express the Ca^{2+}-indicator GCaMP3[11] in pyramidal cells; a chronic mouse preparation for time-lapse imaging of CA1 over weeks[12]; and a miniaturized (<2 g) microscope for Ca^{2+}-imaging in hundreds of cells in freely behaving mice[13]. We thereby tracked somatic Ca^{2+} dynamics of 515–1040 pyramidal cells in individual mice as they repeatedly visited a familiar track over 45 days.

*Authors contributed equally.

Author contributions: YZ, LDB, and MJS designed experiments. YZ, LDB, and EOH acquired data. LDB and LJK analyzed data. LDB, EDC, and KKG built equipment. YZ, LDB, LJK and MJS wrote the paper. AEG and MJS supervised the research

We first verified CA1 neurons' place coding attributes as mice explored various arenas. The data revealed up to 740 cells (range: 73–740 cells; n = 13 mice) undergoing Ca^{2+} excitation in single fields of view (Fig. 1b–d; Supplementary Fig. 1; and Movie 1). Ca^{2+} dynamics generally displayed quiescent periods interrupted by prominent transients. This concurs with *in vitro* studies showing GCaMP3 reports spike bursts well but for solitary spikes has weak signals easily masked by background fluorescence or noise[11]. We used established computational means[14] to extract individual cells and their dynamics from each session's Ca^{2+}-imaging data, without regard to mouse behavior (**Online Methods**).

As expected of place cells, during active exploration many pyramidal cells exhibited Ca^{2+}-excitation when the mouse occupied a specific portion of its arena (Fig. 1d). When we placed mice in two different arenas at the same location in the room but with distinct shape, color and orientation cues, a subset of cells exhibited re-mapping[2], showing spatially distinct patterns of Ca^{2+}-excitation in the two arenas. Consistent with prior work, some cells had place fields in only one arena. Thus, one can optically detect CA1 place cell activity in freely behaving mice, in accord with a Ca^{2+}-imaging study in mice exploring a virtual reality[15].

To study place cells over weeks, we trained mice to run back and forth on a linear track; Ca^{2+}-imaging occurred on ten sessions over 45 days (Fig. 2a). As in prior studies in linear environments[16], many cells had clear place-coding properties that usually depended strongly on the mouse's running direction (Fig. 2b–d). Overall, ∼90% of cells had at least one Ca^{2+} transient during running.

For detailed analyses we focused on a subset of mice (n = 4) and used a conservative definition of place field by requiring statistically significant mutual information between a cell's Ca^{2+} excitation events and the mouse's location[17]. With this definition, ∼20% of cells had place fields for left, right, or both running directions (Fig. 2c–e). The set of place fields fully covered the track, with the ends represented more densely than the interior (Fig. 2f,g). The mean place field size was ∼27% of the 84-cm track, within the range published for mice[15,16,18,19]. For each place field we detected Ca^{2+} activity in 17 ± 14% of running passes (n = 1656 place fields, mean ± s.d.; range: 2-87%). Across days 5–35 the percentages of cells on each day with place fields for right (12 ± 1%; mean ± s.e.m) or left (12 ± 1%) motion did not vary (Kruskal-Wallis ANOVA; P = 0.77 and 0.88 for right and left, respectively; n = 7 sessions; n = 4 mice) (Fig. 2e). Nor were there changes in the distributions of place fields' locations or sizes (Fig. 2g,h) (Kolmogorov-Smirnov test; P=0.06–0.99 for locations and 0.02–0.99 for sizes, both compared to a significance threshold of $2.4 \cdot 10^{-3}$ that includes the Dunn-Sidák correction for the 21 pairwise comparisons). Notably, we saw no discernible changes to cells' morphologies nor substantial changes in mean Ca^{2+}-transient amplitudes or baseline fluorescence within or across sessions (Supplementary Fig. 2). Thus, photobleaching was negligible, and neither GCaMP3 expression nor illumination had perceptibly deleterious effects on cell health.

To register repeated observations of individual cells, we first examined the precision of image registration (Supplementary Fig. 3). Bootstrap analyses showed errors in aligning cells' locations across sessions were <1 μm. This precision more than sufficed, as even the

closest cells had ≥6 μm between centroids. Over the full study each mouse yielded 515–1040 cells (n = 4 mice), more than the maximum (740) seen in one session but consistent with anatomical data.

A majority of cells was active in one or two sessions (57 ± 1%; mean ± s.d.; n = 2960 cells; n = 4 mice). 2.8 ± 0.3% were active in all 10 sessions (Fig. 3a,b). Yet, each session had the same percentage (31 ± 1%) of active cells out of the full tally (Kruskal-Wallis ANOVA; P = 0.46) (Fig. 3b *inset*). Cells came in and out of this active subset day-by-day, but the overlap in active subsets from any two days was only moderately time-dependent, declining from ∼60% for sessions 5 days apart to ∼40% for 30 days apart (Fig. 3c).

Comparisons between any two sessions revealed ∼15–25% overlap in the subsets of cells with statistically significant place fields, declining from ∼25% for sessions 5 days apart to ∼15% for 30 days (Fig. 3c). Notably, when individual cells did show place fields in more than one session, the place fields' locations were generally identical (Fig. 3d). This is a compelling, independent validation of our image registration protocol. Though cells came in and out of the place-coding ensemble, place fields' invariant locations plus the slowly declining overlap in place-coding ensembles led to spatial representations that retained a clear resemblance while decaying over time (Fig. 3e–g).

We next sought factors that influenced cells' recurrences in the place-coding ensemble. If cell physiological or coding parameters were key influences, Ca^{2+}-activity or place-coding parameters might correlate with recurrence probabilities. But if network dynamics were more important, the data might reveal no relationships between cells' characteristics and recurrence probabilities. Notably, the numbers of sessions in which cells had Ca^{2+} activity or statistically significant place fields were uncorrelated with their rates and amplitudes of Ca^{2+} activation (Supplementary Fig. 4). Cells with high place-coding stability in single sessions had virtually the same recurrence odds as other cells (Supplementary Fig. 5). Neither inclusion of Ca^{2+} transient amplitudes in the computations of place fields nor variations in how we extracted cells from the raw data altered these findings (Supplementary Figs. 6, 7). Overall, we failed to find parameters predictive of which cells recur in either the active or place-coding ensembles.

Given place fields' invariant locations, did the ∼15–25% overlap between different days' coding ensembles suffice to retain a stable spatial representation? To address this, we used Bayesian decoding techniques to study how well we could reconstruct the mouse's location from the Ca^{2+}-imaging data (Supplementary Fig. 8 and Fig. 3h–j). We created a set of decoders of a common mathematical structure, trained each decoder on a portion of one day's data, and tested it on other data. When test and training data were from the same day, estimates of mouse location were excellent (median error nearly always <7 cm) and highly significant compared to shuffled test data ($P<10^{-160}$; Kolmogorov-Smirnov test). We then asked how well a decoder trained on data from one day would perform on data from other days. In comparisons between decoders using the same number of cells, performance declined only modestly with the interval between training and testing and remained very significant for 30-day intervals ($P=10^{-27}$; Kolmogorov-Smirnov test). Thus, the ∼15%

commonality in place-coding subsets across 30 days sufficed to deduce the mouse's trajectory using a decoder trained on data of 30 days prior.

Though GCaMP3 does not faithfully report single spikes[11], our approach can sense isolated spike bursts. To evade analyses of place coding by using only solitary spikes, cells would have to avoid burst spiking across entire sessions while still encoding spatial information. We do not exclude this possibility but consider it unlikely, especially given the key place coding role ascribed to bursts[20] and lack of correlation here between cellular Ca^{2+} activity and involvement in place coding. Improved Ca^{2+} sensors should reveal a greater portion of spiking activity and could amend our findings with GCaMP3. Our general approach will allow long-term tracking of large neural ensembles in multiple brain areas beyond CA1.

Overall, our data indicate retention of spatial information in CA1 combines stable place field locations with ∼15–25% odds an individual cell will recur in the ensemble place code. Prior long-term recordings had stressed place field stability and usually focused on tens or fewer cells, far less than the ∼3500 we studied. *In vivo* imaging allows reliable tracking of CA1 cells over months[12], here revealing the fluctuating membership of place coding ensembles. This supports prior reports of individually stable place fields but shows CA1 coding has day-to-day dynamism at the cellular level while preserving spatial information in the ∼15–25% overlap between coding ensembles from any two days. Conversely, each episode in a familiar arena has a unique signature via the ∼75–85% of cells that do not overlap when comparing coding ensembles from any two sessions (Fig. 3c). Note that our data show the existence of these non-overlapping signatures but do not imply any functional significance. One possibility is that coding turnover is a long-term form of the spike-rate re-mapping seen over shorter intervals[2] and might help distinguish traces of distinct events occurring in the same environment.

Online Methods

Viral vector

University of North Carolina Vector Core packaged AAV2/5 vectors (∼$2{\cdot}10^{12}$ particles/mL) expressing GCaMP3 via the CaMKIIα promoter[21]. We used immuno-staining of virally infected CA1 tissue to verify GCaMP3 and CaMKII co-expression in the same cells.

Mice

Stanford APLAC approved all procedures. Male C57/BL6 mice (aged 8–12 weeks at start, housed 2–3 per cage with a running wheel) underwent two procedures under isoflurane (1.5–2%). We first injected AAV2/5-CaMKIIα-GCaMP3[11,15] (250 nL) into CA1 (–1.9 mm from Bregma, 1.4 mm mediolateral, –1.65 mm dorsoventral). A week after viral transduction we implanted a glass guide tube just dorsal to CA1, as described[12].

Ca^{2+}-imaging

We used the integrated microscope as described for imaging CA1[13], with minor adaptations for time-lapse studies[12,22]. The first session (∼4 weeks after second surgery) began by installing the microendoscope into the guide tube of isoflurane-anesthetized mice, guided by

two-photon imaging of CA1 through the microendoscope[12,22,23]. The microendoscope was a gradient refractive index lens (GRINtech GmbH, 0.44 pitch length, 0.47 NA) and relayed light from CA1 to a focal plane outside the mouse. After verifying GCaMP3 expression, we fixed the microendoscope in the tube using UV-curing adhesive (Norland, NOA 81).

We lowered the integrated microscope towards the microendoscope until we saw GCaMP3 fluorescence using the microscope's LED light source (0.05–0.2 mW). After finding a suitable imaging site, we attached to the cranium the microscope's base plate using dental acrylic and Cerebond. This plate stayed with the mouse even when the microscope was detached. We generally darkened the acrylic with carbon powder (Sigma, 484164).

Mice displayed vigorous activity ∼1–2 min after release from anesthesia. We chose isoflurane for its rapid clearance from tissue but nevertheless waited 20–30 min before imaging. Illumination (<0.4 mW) lasted ∼3 min per imaging trial. Each session on the track involved 4–7 trials, over which the mouse usually ran >100 roundtrip passes. During ∼3 min between trials the mouse rested in a holding chamber. After all trials we waited another 10–15 min, then briefly (∼5 min) re-anesthetized the mouse to detach the microscope. A typical session yielded <25 min of video (19.9 Hz; 480 × 480 pixels covering ∼0.34 mm^2 of CA1).

In following sessions we re-attached the microscope to its base while the mouse was isoflurane-anesthetized (∼5 min), then waited 20–30 min before imaging. We verified the field of view matched prior sessions or made slight focal adjustments[13]. Subsequent steps were as above.

Behavioral analysis

During Ca^{2+}-imaging the mouse explored: a square 46 × 46 × 15 cm^3 arena (acrylic); a circular arena (21-cm-radius; red plastic); or an 84 × 4.5 × 4.5 cm^3 elevated linear track (aluminum). For three days prior to Ca^{2+}-imaging on this track we trained water-scheduled mice to run back and forth for water rewards at the ends. An overhead camera (Prosilica, EC640) recorded this behavior, using infrared LEDs (Lorex, VQ2120) and dim room lights for illumination.

We analyzed videos using MATLAB (Mathworks) and set all pixels to zero or one if their intensities were, respectively, above or below 10% of the median intensity. This demarcated the mouse due to its dark fur. We determined the mouse's position as the centroid of each binary image and calculated its velocity after smoothing the position data (0.5 s sliding average).

Basic processing of Ca^{2+}-imaging videos

Analysis used ImageJ (NIH) and MATLAB routines. Since the microscope's sensor had a Bayer color filter[13], we zeroed all pixels in the red and blue channels and de-mosaiced GCaMP3 signals in the green pixels by Bayer interpolation using the MATLAB function demosaic(). Image rows were readout successively; to correct for the slightly variable number of LED pulses illuminating each row we normalized each demosaiced pixel by the mean intensity in its row. The illumination exhibited mild spatial non-uniformity, so we also

normalized each pixel by the ratio of the mean intensity along its column to that of a reference column. We coarse-grained images to 240 × 240 pixels each the mean of four pixels at the finer density.

We used rigid image registration to correct lateral displacements of the brain. We created an image stack, $F_2(t)$, as the difference between the original stack, $F(t)$, and a smoothed version of $F(t)$ (20-pixel-radius smoothing filter). Within $F_2(t)$ we selected a high-contrast sub-region to provide a fiducial marker. To mutually register all frames of $F_2(t)$ we used an ImageJ plug-in based on the TurboReg algorithm[24]. For each registered frame of $F_2(t)$ we applied the same coordinate transformation to $F(t)$, yielding the registered stack $F'(t)$.

Identification of neurons

As typical for Ca^{2+}-imaging, we re-expressed registered images as relative changes in fluorescence, $\Delta F'(t)/F'_0 = (F'(t) - F'_0)/F'_0$, where F'_0 is the mean image obtained by averaging the entire movie. We identified spatial filters corresponding to individual cells using an established cell sorting algorithm that applies principal and independent component analyses[13,14,25]. Cells' spatial filters were based on Ca^{2+} activity (temporally down-sampled 4×) over the entire session, not just when the mouse was running. For each filter we zeroed all pixels with values <50% of that filter's maximum intensity.

Detection of Ca^{2+}-transients

We used each cell's thresholded spatial filter to extract its Ca^{2+} activity from the $\Delta F'(t)/F'_0$ stack. We removed baseline fluctuations (ascribed to Ca^{2+} activity outside the focal plane or in neuropil) by subtracting the median trace (200 time bins sliding window) and applied a 5-frame (∼250 ms) sliding average. We identified Ca^{2+}-transients by searching each trace for local maxima that had: (1) Peak amplitude more than two standard deviations (2σ) from the trace's baseline; (2) ≥10 frames (∼0.5 s) when the mean intensity surrounding the peak was >2σ; (3) Separation of >6 frames (∼300 ms) from adjacent Ca^{2+}-transients. We set a Ca^{2+}-transient's occurrence to the temporal midpoint in the rise to peak fluorescence from the most recent trough, approximating a time midway within the corresponding spike burst. To correlate Ca^{2+} activity to mouse behavior, we offset Ca^{2+}-transient occurrences by ∼250 ms due to GCaMP3's known delayed response[11].

On ∼7% of all detected Ca^{2+}-transients, fluorescence increases occupied more pixels than a single spatial filter. To mitigate effects of this spillover we took a conservative approach, allowing only one cell among a group of neighbors to register a Ca^{2+}-transient within a ∼250 ms window. We defined neighbors as cells whose spatial filters had non-zero pixels within 30 μm of each other. If multiple Ca^{2+}-transients arose within ∼250 ms among neighboring cells, we retained only the transient with the greatest peak $\Delta F'(t)/F'_0$ value.

Registration of cells across sessions

We mapped all cells from each session by assembling their thresholded spatial filters onto a single image. Picking one day's map for reference (usually day 15), we aligned the others to this via a scaled image alignment using TurboReg[24] (Supplementary Fig. 3a). This corrected

slight translations, rotations, or focus-dependent magnification changes between sessions and yielded each cell's location in the reference coordinate system.

Next, we visually identified candidate cells across sessions that might be the same neuron seen on multiple occasions. We applied two observations: our registration procedures had sub-micron precision (Supplementary Fig. 3b–e); the distance between centroids of neighboring somata was always >6 μm (Supplementary Fig. 3f). We thus considered a candidate set of cells to be the same neuron if all pair-wise separations were ≤6 μm. If any of the pair-wise separations exceeded 6 μm we split the set into two or more.

Place fields

To analyze place fields we identified ‘movement periods’ when the mouse ran continuously >0.5 cm/s. Additionally, in open field arenas the speed had to exceed 1 cm/s at some point during the movement; on the track it had to transiently exceed 9.2 cm/s. These criteria rejected small movements such as grooming, rearing, or head-turning.

On the linear track we considered 3.5-cm spatial bins and excluded the last 7 cm at each end where water rewards were given. In open field arenas, bins were 4 cm^2. We divided the number of Ca^{2+} transients in each bin by the mouse's total occupancy time there, applied a Gaussian smoothing filter (linear track: $\sigma = 8.75$ cm; open field: $\sigma = 3.5$ cm), and normalized each place field by its maximum value. On the track we separately considered place fields for left and right running directions. The number of bins in which a place field had a value ≥50% of its maximum determined the place field's width. We tabulated each place field's position as its centroid.

Statistical analysis

For each place field (calculated for one running direction) we computed the mutual information[26] between Ca^{2+}-transients and the mouse's location (7-cm bins). We also performed 10,000 distinct shuffles of the Ca^{2+}-transient times and calculated the mutual information for each shuffle. This yielded the *P*-value of the true mutual information relative to the shuffles. $P \leq 0.05$ indicated a significant place field for that running direction.

To generate the null hypothesis for place fields' displacements between a pair of days, we used the place fields' measured locations but shuffled cells' identities on each of the days. We calculated the distribution of all displacements, averaged over 1000 distinct pairs of shuffles. Fig. 3e shows the mean null hypothesis curve found by averaging over all pairs of days.

Decoding

We used Bayesian methods[27,28] to estimate mouse location based on cells' Ca^{2+}-transients. Details are in Supplementary Fig. 8.

Supplementary Material

Refer to Web version on PubMed Central for supplementary material.

Acknowledgments

We thank L. Looger for GCaMP3 plasmid and A. Attardo, T. Davidson, J. Fitzgerald, J. Li, J.Z. Li, A. Lui, C. Ramachandran, O. Yizhar, and T. Zhang for helpful conversations and assistance. We appreciate fellowships from Stanford (LDB, EOH, LJK), NSF (LDB, LJK), Simons (LJK), Machiah (YZ), and Rothschild Foundations (YZ), and research funding to MJS from the Paul G. Allen Family Foundation, NIMH, NIA, and an NIH Director's Pioneer award.

References

1. O'Keefe, JNL. The Hippocampus as a Cognitive Map. Clarendon Oxford; 1978.
2. Leutgeb S, et al. Independent codes for spatial and episodic memory in hippocampal neuronal ensembles. Science. 2005; 309:619–623. 309/5734/619 [pii] 10.1126/science.1114037. [PubMed: 16040709]
3. Buzsaki G. Large-scale recording of neuronal ensembles. Nat Neurosci. 2004; 7:446–451. 10.1038/nn1233 nn1233 [pii]. [PubMed: 15114356]
4. Muller RU, Kubie JL, Ranck JB Jr. Spatial firing patterns of hippocampal complex-spike cells in a fixed environment. J Neurosci. 1987; 7:1935–1950. [PubMed: 3612225]
5. Thompson LT, Best PJ. Long-term stability of the place-field activity of single units recorded from the dorsal hippocampus of freely behaving rats. Brain Res. 1990; 509:299–308. 0006-8993(90)90555-P [pii]. [PubMed: 2322825]
6. Kentros C, et al. Abolition of long-term stability of new hippocampal place cell maps by NMDA receptor blockade. Science. 1998; 280:2121–2126. [PubMed: 9641919]
7. Lever C, Wills T, Cacucci F, Burgess N, O'Keefe J. Long-term plasticity in hippocampal place-cell representation of environmental geometry. Nature. 2002; 416:90–94. 10.1038/416090a 416090a [pii]. [PubMed: 11882899]
8. Kentros CG, Agnihotri NT, Streater S, Hawkins RD, Kandel ER. Increased attention to spatial context increases both place field stability and spatial memory. Neuron. 2004; 42:283–295. S0896627304001928 [pii]. [PubMed: 15091343]
9. Cacucci F, Wills TJ, Lever C, Giese KP, O'Keefe J. Experience-dependent increase in CA1 place cell spatial information, but not spatial reproducibility, is dependent on the autophosphorylation of the alpha-isoform of the calcium/calmodulin-dependent protein kinase II. J Neurosci. 2007; 27:7854–7859. 27/29/7854 [pii] 10.1523/JNEUROSCI.1704-07.2007. [PubMed: 17634379]
10. Muzzio IA, et al. Attention enhances the retrieval and stability of visuospatial and olfactory representations in the dorsal hippocampus. PLoS Biol. 2009; 7:e1000140.10.1371/journal.pbio.1000140 [PubMed: 19564903]
11. Tian L, et al. Imaging neural activity in worms, flies and mice with improved GCaMP calcium indicators. Nat Methods. 2009; 6:875–881. nmeth.1398 [pii] 10.1038/nmeth.1398. [PubMed: 19898485]
12. Barretto RP, et al. Time-lapse imaging of disease progression in deep brain areas using fluorescence microendoscopy. Nat Med. 2011; 17:223–228. nm.2292 [pii] 10.1038/nm.2292. [PubMed: 21240263]
13. Ghosh KK, et al. Miniaturized integration of a fluorescence microscope. Nat Methods. 2011; 8:871–878. nmeth.1694 [pii] 10.1038/nmeth.1694. [PubMed: 21909102]
14. Mukamel EA, Nimmerjahn A, Schnitzer MJ. Automated analysis of cellular signals from large-scale calcium imaging data. Neuron. 2009; 63:747–760. S0896-6273(09)00619-9 [pii] 10.1016/j.neuron.2009.08.009. [PubMed: 19778505]
15. Dombeck DA, Harvey CD, Tian L, Looger LL, Tank DW. Functional imaging of hippocampal place cells at cellular resolution during virtual navigation. Nat Neurosci. 13:1433–1440. nn.2648 [pii] 10.1038/nn.2648. [PubMed: 20890294]
16. McHugh TJ, Blum KI, Tsien JZ, Tonegawa S, Wilson MA. Impaired hippocampal representation of space in CA1-specific NMDAR1 knockout mice. Cell. 1996; 87:1339–1349. S0092-8674(00)81828-0 [pii]. [PubMed: 8980239]

17. Markus EJ, Barnes CA, McNaughton BL, Gladden VL, Skaggs WE. Spatial information content and reliability of hippocampal CA1 neurons: effects of visual input. Hippocampus. 1994; 4:410–421.10.1002/hipo.450040404 [PubMed: 7874233]
18. Nakazawa K, et al. Hippocampal CA3 NMDA receptors are crucial for memory acquisition of one-time experience. Neuron. 2003; 38:305–315. [PubMed: 12718863]
19. Rotenberg A, Mayford M, Hawkins RD, Kandel ER, Muller RU. Mice expressing activated CaMKII lack low frequency LTP and do not form stable place cells in the CA1 region of the hippocampus. Cell. 1996; 87:1351–1361. [PubMed: 8980240]
20. Lisman JE. Bursts as a unit of neural information: making unreliable synapses reliable. Trends Neurosci. 1997; 20:38–43. S0166-2236(96)10070-9 [pii] 10.1016/S0166-2236(96)10070-9. [PubMed: 9004418]
21. Gradinaru V, et al. Targeting and readout strategies for fast optical neural control in vitro and in vivo. J Neurosci. 2007; 27:14231–14238. 27/52/14231 [pii] 10.1523/JNEUROSCI.3578-07.2007. [PubMed: 18160630]
22. Barretto RP, Messerschmidt B, Schnitzer MJ. In vivo fluorescence imaging with high-resolution microlenses. Nat Methods. 2009; 6:511–512. nmeth.1339 [pii] 10.1038/nmeth.1339. [PubMed: 19525959]
23. Barretto, RPJ.; Schnitzer, MJ. Imaging: A Laboratory Manual. Yuste, R., editor. Cold Spring Harbor Laboratory press; 2011. Ch 50
24. Thevenaz P, Ruttimann UE, Unser M. A pyramid approach to subpixel registration based on intensity. IEEE Trans Image Process. 1998; 7:27–41.10.1109/83.650848 [PubMed: 18267377]
25. Nimmerjahn A, Mukamel EA, Schnitzer MJ. Motor behavior activates Bergmann glial networks. Neuron. 2009; 62:400–412. S0896-6273(09)00244-X [pii] 10.1016/j.neuron.2009.03.019. [PubMed: 19447095]
26. Shannon CEWW. The mathematical theory of communication. University of Illinois Press, Urbana, Illinois. 1949
27. Brown EN, Frank LM, Tang D, Quirk MC, Wilson MA. A statistical paradigm for neural spike train decoding applied to position prediction from ensemble firing patterns of rat hippocampal place cells. The Journal of neuroscience: the official journal of the Society for Neuroscience. 1998; 18:7411–7425. [PubMed: 9736661]
28. Quian Quiroga R, Panzeri S. Extracting information from neuronal populations: information theory and decoding approaches. Nature reviews Neuroscience. 2009; 10:173–185.10.1038/nrn2578 [PubMed: 19229240]

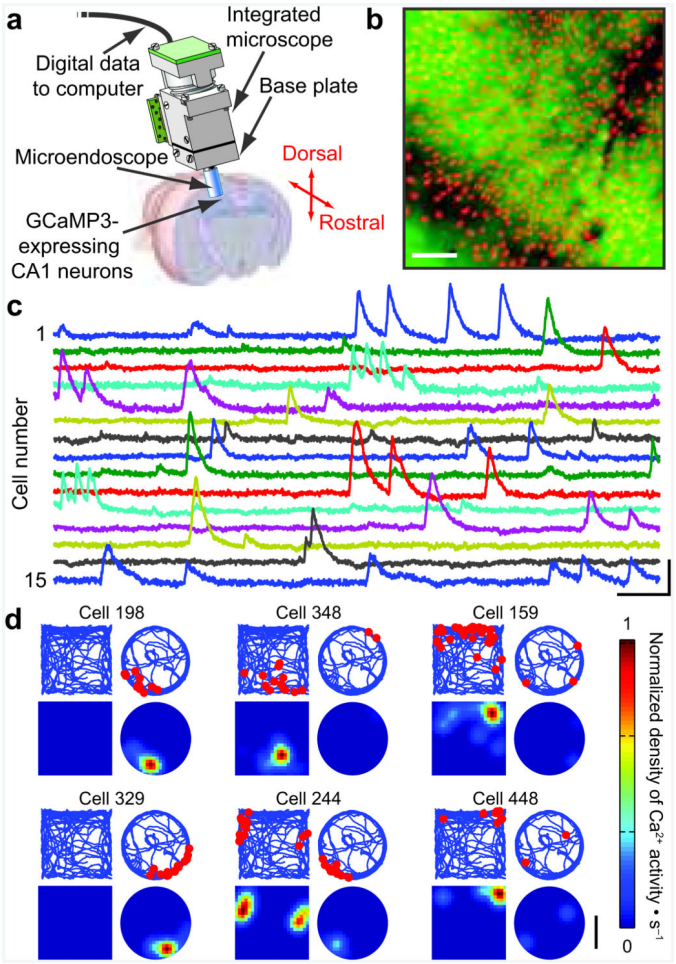

Figure 1. Ca^{2+}-imaging in hundreds of place cells in freely behaving mice

(a) A tiny microscope equipped with a microendoscope images pyramidal cells expressing GCaMP3 via control of a CaMKIIα promoter. The microscope's base plate is fixed to the skull, for repeated imaging of the same cells.

(**b**) 705 cells (red somata) identified by Ca^{2+}-imaging in a behaving mouse (Movie 1), atop a mean fluorescence image (green) of CA1. Blood vessels appear as shadows.

(**c**) Relative fluorescence changes ($\Delta F/F$) for 15 of the cells in **b**.

(**d**) Spatial distributions of the mouse's location during Ca^{2+} excitation, for 6 example cells in a mouse that explored two distinct arenas. *Upper panels*, blue lines show the mouse's trajectory; red dots mark the mouse's position during Ca^{2+} events. *Lower panels*, Gaussian-smoothed (σ = 3.5 cm) density maps of Ca^{2+} events, normalized by the mouse's occupancy time per unit area and the cell's maximum response in the two arenas. Scale bars: 100 μm in **b**; 10 s (horizontal) and 5% $\Delta F/F$ (vertical) in **c**; 20 cm in **d**.

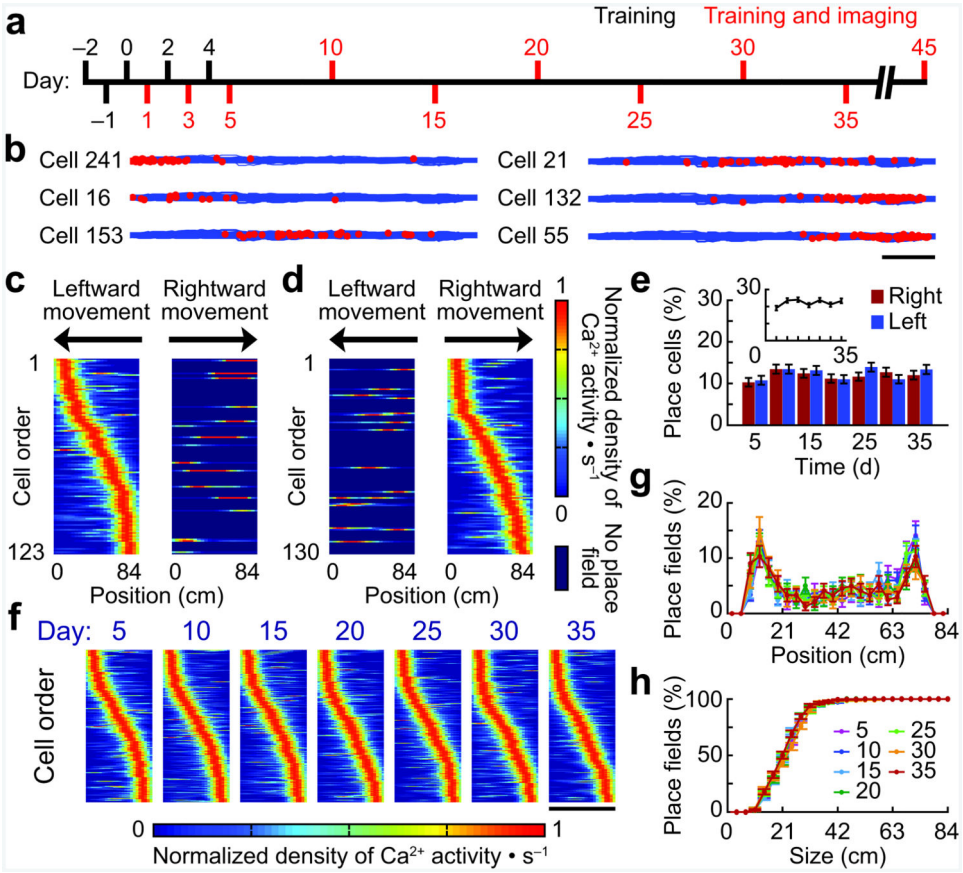

Figure 2. Basic aspects of CA1 place codes are stable over weeks

(**a**) Mice trained to run back and forth on a linear track (days in black). During Ca^{2+}-imaging sessions (red), the mice performed the same behavior.

(**b**) The mouse's trajectory (blue lines) and its locations during cellular Ca^{2+} excitation (red dots) illustrate place cell activity.

(**c**, **d**) Gaussian-smoothed (σ = 8.75 cm) maps of Ca^{2+} activity on the track, shown for the subsets of cells on Day 15 with statistically significant place fields during left, **c**, or right, **d**, motion. 85–93% of cells had a place field for one direction only; dark blue marks the lack of a place field for the other direction. Cells from four mice are pooled, ordered by place fields' centroid locations. Ca^{2+} maps are normalized by each cell's maximum activity during left, **c**, and right, **d**, motion.

(**e**) The fraction of cells with statistically significant place fields, expressed as a percentage of cells found in each session (mean ± s.e.m.; 807–1000 total cells per day; *n* = 4 mice), was constant over the study for each motion direction (colored bars) and in total (*inset*).

(**f**) The ensemble of all place fields found in each session covered the entire track. Place fields are shown as smoothed maps of Ca^{2+} excitation as in **c** and **d**, ordered by centroid location on each day and pooled across four mice and both movement directions.

(**g**) Spatial distributions of place fields' centroid locations were constant over 1 mo. Place fields' centroids were tallied in 3.5-cm bins (mean ± s.e.m; *n* = 4 mice; 178–268 cells per day). Color key is the same as for **h** and indicates the day of imaging.

(**h**) Cumulative distributions of place fields' widths did not evolve (mean ± s.e.m). Place fields had a median (± 33% confidence interval) width of 24 ± 3.5 cm.
Scale bars: 10 cm in **b**; 84 cm in **f**.

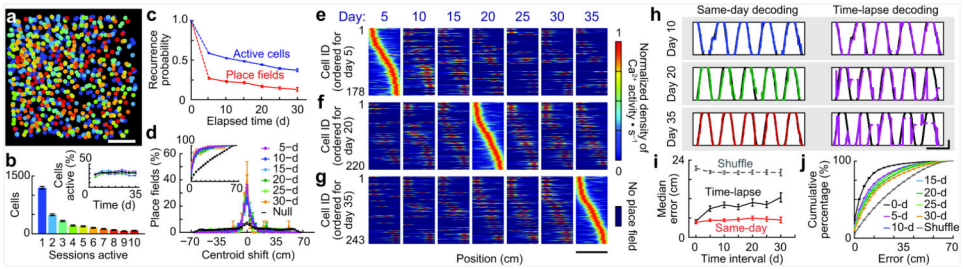

Figure 3. Place fields are spatially invariant and temporally stochastic while preserving a stable representation at the ensemble level

(**a**) 826 cells showed Ca^{2+} activity in one mouse over 45 days. Number of sessions in which each cell was active is shown via the color scheme in **b**.

(**b**) Histogram of number of sessions in which each of 2960 cells from 4 mice was active. Error bars show s.d. from counting statistics. *Inset*: A constant fraction of all cells detected over 10 sessions was active each day. Colored data are from individual mice. Mean ± s.e.m is in black.

(**c**) If a cell had Ca^{2+} activity in one session, the odds (blue data; mean ± s.e.m) it also had Ca^{2+} activity in a subsequent session declined with the elapsed time interval. If a cell had a statistically significant place field in one session, the odds (red data) it had a place field in a subsequent session also declined with time.

(**d**) If they reappeared, place fields generally did not shift their centroid locations. Distributions of centroid shifts (colored by days between sessions; mean ± s.e.m.) were indistinguishable (Kolmogorov-Smirnov test; $P \geq 0.17$), sharply peaked at zero, and highly distinct from the null hypothesis place fields would randomly re-locate ($P = 4 \cdot 10^{-67}$; Kolmogorov-Smirnov test). *Inset*: Cumulative histograms of shift magnitudes. 74–83% were ≤7 cm. Median shift (3.5 cm) was much less than the median place field width (24 cm).

(**e–g**) Place field maps for cells found on multiple days, ordered by place fields' centroid positions on day 5 (**e**), day 20 (**f**), or day 35 (**g**), reveal continuous evolution of the ensemble representation of space. Data pooled across 4 mice.

(**h**) Time-lapse decoders retain substantial accuracy over 30 days. Reconstructions of the mouse's trajectory (colored curves) and its actual position (black curves). Three paired reconstructions compare: *Right*, time-lapse decoders trained on data from day 5, using all cells with place fields on both days of each pair; *Left*, decoders trained on data from the same day as the test trial. Each pair uses an equal number of cells, optimally chosen in *left* to minimize errors.

(**i**) Median errors in estimating the mouse's position are ∼7–13 cm (black points; mean of the median errors ± s.e.m.), even for decoders trained on data from 30 days prior. Red points are for decoders trained on data from the same day as test data, using equal numbers of cells as black points and optimally chosen to minimize errors. Gray points are errors using shuffled traces of Ca^{2+} activity from the same day as training data (averaged over 10,000 shuffles).

(**j**) Cumulative distributions of decoding error magnitudes (mean ± s.e.m.). Black curve: Test and training data from same day. Colored curves: Test data 5-30 days apart from that used for training. Gray curve: Decoders tested on shuffled data.

Scale bars: 100 μm in **a**; 84 cm in **e–g**; 2 s (horizontal) and 10 cm (vertical) in **h**.